BROWNIAN CIRCUIT SAMPLING FOR CROSS ENTROPY BENCHMARKING

Michael Sizemore, Gregory Bentsen

Department of Physics, William & Mary

April 6, 2026

Abstract

Cross-entropy benchmarking (XEB) has been a prominent figure of merit for random circuit sampling (RCS) quantum advantage tests for the past decade. While high scores on the simplest form of XEB are classically achievable, the metric still warrants study as a diagnostic for random quantum circuit performance in the presence of realistic noise channels in near-term hardware. However, analytic work on XEB has proved difficult due to the intractability of existing theoretical tools focused on discrete random circuit models, especially past the case of linear order XEB. To address this issue, we present Brownian random circuit sampling, which addresses these concerns and makes future exploration into XEB measures much simpler. We model random unitary gates as all-to-all Brownian 2-body gates with couplings obeying a Gaussian distribution. By disorder-averaging over these couplings, we can derive a partition function expression for the output-averaged linear XEB, enabling a statistical mechanics treatment. We explore how the addition of noisy corrections to this partition function breaks the underlying symmetries of this model, the impact of which can be both derived and explained via mean-field theory. This paper establishes a set of theoretical tools that will be extended to more complicated cases in forthcoming work.

Introduction

Since the conceptualization of quantum computing a half-century ago[1], a major area of research has been the development of tasks and benchmarks for these computers. These can both compare performance to classical machines and provide experimentally relevant metrics of noise resilience, both of which are key for machines in the current era of noisy intermediate-scale quantum (NISQ) computing[2]. One of the canonical examples of this is random circuit sampling (RCS), a task relying on quantum chaos that is difficult to simulate on classical processors. RCS was the foundation of one of the first widely publicized results in experimentally realizable quantum advantage on Google's Sycamore processor[3], using a formalism called cross-entropy benchmarking (XEB)[4] to compare to the best available classical results in reconstructing the output probability distribution of a brickwork circuit of random unitary gates. However, it is unclear whether XEB-type measures can genuinely certify quantum advantage. For example, in the Sycamore case, the claimed

quantum speedup was as high as millennia in the largest considered case, but these results were rapidly mitigated[5] and later work demonstrated that classical algorithms could produce good XEB marks at linear order without the need to obtain samples from genuine quantum hardware[6]. Further research is needed to investigate XEB measures for near-term quantum advantage verification in the pre-fault tolerance era.

Additionally, there remains gaps in the literature regarding the analytic structure of XEB measures. While such measures can be computed with tools from random matrix theory for an infinite depth circuit, the conventional models of the field (usually built using discrete random circuits) lack the analytical tractability to allow for systematic study of higher-order benchmarks such as nonlinear cross-entropy. It is for this reason that most work on XEB only considers the lowest moments, which limits our *a priori* understanding observed XEB trends generically, and thus limits the utility of XEB as a measure.

This work proposes addressing these problems by replacing the brickwork of random unitaries with an all-to-all unitary evolution in continuous time, based on random 2-body interactions with a zero-mean, Gaussian distributed random couplings[7,8]. The appeal of this method is that it maps finite-depth random circuit calculations onto a statistical mechanics problem that we can treat with mean-field theory and saddle point evaluation. The impact of this is threefold: First and most importantly, it enables the calculation of nonlinear XEB moments for a finite-depth circuit, a unique feature of this model. Second, it introduces a finite depth T as a continuously tunable parameter, which allows us to model measures like XEB for both shallow-depth and large-depth circuits within the same framework. Third, the simplicity of this formalism allows for incorporating corrections such as common noise channels and higher-body interactions with ease. We additionally discuss and apply the diagrammatic language of random matrix theory by adapting it for saddle point classification, which makes behaviors such as symmetry breaking and phase transitions clear and visually intuitive. The explanation and development of these methods enables for both forthcoming analytical calculations as well as ease of modification to incorporate more exotic noise channels and higher order XEB moments into analytically tractable models that are beyond the reach of other theoretical tools. This opens the door to further studies on how real-world factors can impact the behavior of these metrics.

Background Theory

The interest in random unitary circuit sampling as a task for benchmarking quantum computers derives from their chaotic output statistics - in particular, if the probability p of measuring an output string $\langle \mathbf{x}|$ from a circuit U given an input state $|0\rangle$ are $p = |\langle \mathbf{x}| U |0\rangle|^2$, these probabilities are distributed according to the *Porter-Thomas distribution*:

$$\mathcal{P}(p) = de^{-dp} \tag{1}$$

where $d = 2^n$ is the dimension of the Hilbert space considered. This distribution occurs in known chaotic physical systems[9,10], and is a characteristic signature of a chaotic unitary process. Arguments from complexity theory[11] support the idea that the transition probabilities generated by such a circuit are in general exponentially hard to classically predict, as the complexity of simulating quantum chaotic

dynamics on a circuit with fixed n scales exponentially with system size.

Often, RCS modelers will use a discrete circuit that matches these chaotic statistics at low central moments. This low-moment approach works for computing metrics such as averaged linear XEB thanks to this alignment. However, discrete random circuit cannot compute*general* XEB measures, such as a nonlinear XEB moment or flucatuations in the linear XEB. We develop a formal analysis of XEB calculations that address these difficulties with discrete circuit calculations below.

Calculations of random circuit dynamics are facilitated by the "replica trick"[12] and disorder-averaging to manipulate a probability measure into a more tractable form. Say we wish to calculate the first central probability moment of a random circuit U initialized in the all-0 state producing a bitstring $\mathbf{x}$, or $|\langle \mathbf{x}| U |0\rangle|^2$. We now exploit the channel-state duality i.e. the *Choi-Jamiołkowski isomorphism*[12] to recast the probability as a transition amplitude on 2 copies ("replicas") of the system:

$$\begin{aligned} |\langle \mathbf{x}| U |0\rangle|^2 &= \langle \mathbf{x}| U |0\rangle \langle 0| U^\dagger |\mathbf{x}\rangle \\ &= (-1)^{\mathbf{x}} \langle \mathbf{x}\bar{\mathbf{x}}| U \otimes U^{\mathcal{T}} |01\rangle \end{aligned} \tag{2}$$

We can construct a similar form for the XEB. The canonical work behind XEB[4] defines the metric with "cross" denoting the involvement of two probability distributions (the circuit dist. $\mathcal{P}_{\mathcal{U}} = \{p_{U,i}\}_i$ and the sampler dist. $\mathcal{Q} = \{q_i\}_i$) involved:

$$\text{XEB} = -\langle \ln(q_i) \rangle_{p_{U,i}} \tag{3}$$

where i denotes a particular output string. The logarithm can be Taylor expanded to take moments of the XEB; as nonlinear moments are both subleading and may be generically sample-inefficient to find, one often restricts to the linear XEB

$$\text{XEB}_{\text{lin}} = \langle q_i \rangle_{p_{U,i}} \tag{4}$$

The linear XEB over a unitary circuit is given as

$$\text{lXEB} = \langle \langle \mathbf{x}\bar{\mathbf{x}}\mathbf{x}\bar{\mathbf{x}}| V \otimes V^{\mathcal{T}} \otimes U \otimes U^{\mathcal{T}} |0101\rangle \rangle_{U,\mathbf{x}} \tag{5}$$

for a sampler V whose output probabilities are governed by the distribution $\mathcal{Q}$.

We can then compute output-averaged moments by averaging over circuit realizations U and summing over output strings $\mathbf{x}$. When these circuits are drawn from the *circular unitary ensemble (CUE)*, such calculations are done with *Weingarten calculus*[13], involving integrals of matrix ensembles against a suitable measure where the number of unitaries in the integrand corresponds to the number of replicas

$$\int_{\text{CUE}} U_{i_1,j_1} \dots U_{i_k,j_k} U^*_{i'_1,j'_1} \dots U^*_{i'_k,j'_k} dU \tag{6}$$

This procedure which readily generalizes to arbitrarily high replica number $2k$ for computing (for example) central probability moments p^k. For random unitaries, we specifically consider the *Haar measure* as the measure of integration - that is, these matrices are "Haar-random".

It is useful at this point to introduce a diagrammatic representation of what the contributions to the integrals look like for $d \longrightarrow \infty$. Figure 1 illustrates what some of these terms look like for p^3. The circles each represent a replica circuit with dynamics

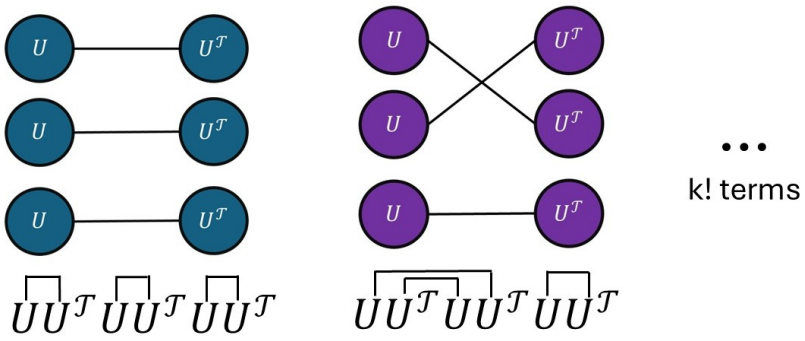

Figure 1: A diagrammatic representation of some random matrix terms. At infinite depth, we can treat the whole random matrix distribution with Weingarten calculus formalism, but existing discrete random circuit models do not admit tractable expressions for higher moments at finite depth.

moving forward in time (U) or time-reversed ($U^{\mathcal{T}}$) - also referred to as"left" or L replicas and "right" or R replicas respectively - and a line between two replicas indicates a nonzero integral over them. Weingarten calculus arguments tell us that we get $k!$ of these states: below each diagram is a notation similar to that of field contractions in quantum field theory, and as in that case our Weingarten integrals ultimately amount to sums over the "contractions" pairing all left and right replicas for which there are $k!$ terms.

While these techniques have found use in studies of quantum chromodynamics as link integrals and in random circuit dynamics, applying to these techniques to discrete circuits is difficult - it is equivalent to exactly solving a Potts model with $k!$ internal state for each spin. This motivated the development of our model, which maintains the Haar-randomness of the generic CUE model while bypassing the intractability of discrete circuit models.

The Brownian Approach

Model Description

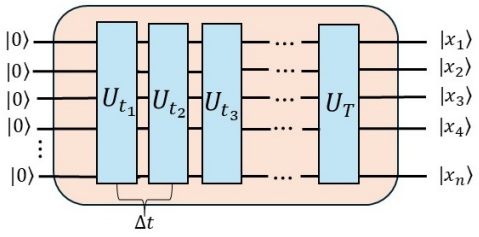

Figure 2: A basic model of an all-to-all Brownian circuit for n qubits with depth T. Note that the timestep Δt is eventually taken to 0, recasting the circuit as a continuous Brownian process.

A circuit schematic of our model is shown in Figure 2. Each unitary layer takes place over a time $t_{i+1} - t_i = \Delta t$, with dynamics controlled by a 2-body time-dependent Hamiltonian

$$H(t) = \sum_{\substack{i<j \\ \alpha,\beta}} J_{ij}^{\alpha\beta}(t)\sigma_i^\alpha \sigma_j^\beta \tag{7}$$

where σ_i^α is the Pauli matrix $\alpha \in \{1, 2, 3\}$ applied to the ith qubit i.e. an operators of the form $I_1 \otimes I_2 \cdots \otimes \sigma_i^\alpha \otimes I_{i+1} \cdots \otimes I_n$. The key to this model is the random couplings $J_{ij}^{\alpha\beta}(t)$, which are Gaussian distributed and have a variance given by

$$\langle J_{ij}^{\alpha\beta}(t) J_{i'j'}^{\alpha'\beta'}(t') \rangle = \delta_{ii'}\delta_{jj'}\delta_{\alpha\alpha'}\delta_{\beta\beta'}\frac{J}{n\Delta t} \tag{8}$$

where J is some real constant. We can then define our circuit as the product of discrete unitary evolutions $U_{t_i} = e^{-iH_i\Delta t}$ such that

$$U = \prod_{i=1}^{T} e^{-iH_i\Delta t} \tag{9}$$

We can combine U and $U^{\mathcal{T}}$ terms by noting that the effect of the time reversal is a sign flip in the Hamiltonian, so we can write

$$H_U = \sum_{\substack{i<j \\ \alpha,\beta}} J_{ij}^{\alpha\beta}(t)(\sigma_{iL}^{\alpha}\sigma_{jL}^{\beta} - \sigma_{iR}^{\alpha}\sigma_{jR}^{\beta}) \tag{10}$$

We can sum over a replica index r ranging from 1 to k to a make a full Hamiltonian we will call H. We are interested in the disorder-averaged lXEB, so we take an expectation value over all circuit configurations:

$$\text{XEB}_{\text{lin}} = \langle \mathbf{x}\bar{\mathbf{x}}\mathbf{x}\bar{\mathbf{x}}| \, \mathbb{E}_J \left(\prod_{i=1}^{T} e^{-iH\Delta t} \right) |0101\rangle \tag{11}$$

As our couplings are Gaussian distributed, the expectation value takes the form of an integral against a Gaussian distribution weighted by the variance given above, which conveniently converts the time evolution into a partition function $e^{-H_{\text{eff}}T}$ with effective Hamiltonian

$$H_{\text{eff}} \approx \frac{J}{2n} \sum_{ra<sb} (-1)^{a+b} \left(\sum_i \vec{\sigma}_{ira} \cdot \vec{\sigma}_{isb} \right)^2 + 9Jn \tag{12}$$

where we have dropped subleading terms in n. Here, $\{a, b\} = \{L, R\}$ and $1 \leq r, s \leq k$ denote choices of replicas, with the restriction $ra < sb$ enforcing that the two choices much be different.

Mean-Field Theory

We can recast the XEB into a path integral via a change of variables, introducing the mean-fields

$$G_{rs}^{ab} = \frac{1}{n} \sum_i \vec{\Omega}_{ira} \cdot \vec{\Omega}_{isb} \tag{13}$$

where the vectors Ω are the Pauli matrices converted into classical spins, and the associated Lagrange multipliers F_{rs}^{ab}. This allows for the construction of an action $I[F_{rs}^{ab}, G_{rs}^{ab}, \Omega_{rs}^{ab}]$, and then applying the large n limits allows for integrating out terms dependent on Ω to leave only $I[F_{rs}^{ab}, G_{rs}^{ab}]$. We can then apply an Euler-Lagrange treatment to force $\frac{\partial I}{\partial G_{rs}^{ab}} = 0$ and substitute in the result. After completing all the algebra, this produces an expression

$$\begin{aligned} I[G_{rs}^{ab}] = &- \sum_i \ln(\langle x_i \bar{x}_i x_i \bar{x}_i \ldots | \exp\left[- \sum_{ra<sb} (-1)^{a+b} J G_{rs}^{ab} T \vec{\sigma}_{ira} \cdot \vec{\sigma}_{isb} \right] |01\ldots\rangle) \\ &+ nT \left[\sum_{ra<sb} \left(-(-1)^{a+b} \frac{J}{2} (G_{rs}^{ab})^2 \right) \right] + 9JnT \end{aligned} \tag{14}$$

where we see the action splits into a matrix element part and a polynomial part. We can approximately evaluate the former by finding the largest eigenvalue $\lambda_{g.s.}$ of the operator in the exponent and then replacing the operator with this eigenvalue. This lets us commute the

exponential past the output state and evaluate the natural log directly, thus yielding $-n\lambda_{g.s.}$.

Saddle Point Analysis

One could exactly diagonalize the matrix part of the action without any consideration of the underlying symmetries at play, but it is instructive to instead use a judicious choice of basis to block-diagonalize and then only exactly diagonalize the singlet subspace. The simplest choice to generate this basis is a generic spin Hamiltonian $H_{\text{spin}} = AS_z + BS^2$ where S is the total "spin" of the system of four replicas, invoking the spectral behavior of a spin addition problem. Taking the eigenstates of this Hamiltonian and then block-diagonalizing yields blocks of size corresponding to the expansion of the tensor product $\mathbf{2} \otimes \mathbf{2} \otimes \mathbf{2} \otimes \mathbf{2} = \mathbf{5} \oplus \mathbf{3^3} \oplus \mathbf{1^2}$ - i.e. each block is a irreducible representation of SU(2). Crucially, the entire effective Hamiltonian is SU(2) invariant, so dynamics within each of these subspaces can be treated separately. In addition, the ground states of H_eff are total spin singlets, so we may restrict our attention to the 2x2 space $\mathbf{1}^2$ which is straightforward to diagonalize to find the largest eigenvalue $\lambda_{\text{g.s.}}$.

When this eigenvalue is substituted into our action, we get an expression $I[J, n, T, G^{ab}_{rs}]$. We can observe that by symmetry we expect exchanging replica pairs to leave our action invariant, and so we can define three cases we wish to consider: the ladder case with mean-fields L, the swap case with mean-fields S, and the vertical case with mean-field V, each of which we can evaluate separately. In the large-n limit, the ground states are the mean field values that extremize the action I. To proceed, we solve the Euler-Lagrange equations of motion $\frac{\partial I}{\partial G} = 0$ which yields saddle point fields $\{L^*, S^*, V^*\}$ and the saddle point action I^* What we find in the case with no noise is that there are two identical ground states where $I = 0, \nabla I = \vec{0}$ at $\{-3, 0, 0\}$ and $\{0, -3, 0\}$ and an excited state with energy $\propto Jn$ at $\{0, 0, -3\}$. This means that, from the perspective of mean-field theory, the contributions to our XEB come equally from the ladder and swap saddle points, combined in the same way one would with different Boltzmann factors in a partition function. This yields the expression

$$\text{XEB} = \frac{2}{2^n}(1 + e^{-24JT})^n \tag{15}$$

which correctly reproduces the infinite-depth value $2/2^n$ as $T \longrightarrow \infty$.

Extensions: Noise and 3-Body Interactions

With the background and model now established, we can now consider extending these tools to realistic problems of interest that feature additional dynamics beyond the simplest 2-body Brownian case considered above. Here we discuss the addition of 3-body interactions and depolarizing noise to the model.

Noise

We begin by considering the impact of two common noise channels on our model: depolarization and over-rotation, applied in the configuration given by Figure 3. The former is given by the Kraus operators

$$E_0 = \sqrt{1 - \frac{3\gamma\Delta t}{4}} I, \qquad E_i = \sqrt{\frac{\gamma\Delta t}{4}} \sigma^i, \tag{16}$$

the effect of which is to isotropically drive each qubit toward the maximally mixed state. As per our noise configuration, turning on this noise breaks exchange symmetry between U and V.

This symmetry breaking likewise breaks the ground state energy - ongoing calculations indicate that the swap saddle point now acquires an energy $\propto \gamma n$. The result is similar for over-rotation: if we introduce a parameter $\mu_{ij}^{\alpha\beta}$ that represents the deviations in the hardware from the ideal coefficients $J_{ij}^{\alpha\beta}$ (and is likewise a Gaussian distributed variable), we in effect shift the 2-body coupling such that the swap saddle point gains the energy $\propto \mu n$.

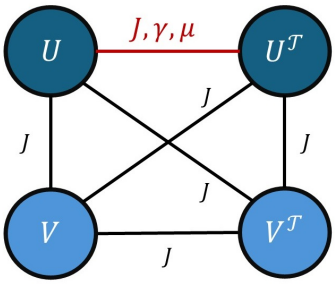

Figure 3: Noise applied on the first run of the "ladder". Note how this breaks the exchange symmetries of the $\gamma, \mu = 0$ case, meaning the ladder and swap saddle points are now longer commensurate.

3-Body Interactions

Another natural extension of our model is to increase the number of qubits that interact in each term of the Brownian Hamiltonian. This is done by simply constructing a Hamiltonian with three Pauli matrices as well as a term with two:

$$H_3 = \frac{M}{2n} \sum_{\substack{i<j<m \\ \alpha\beta\gamma}} \left(\sum_{r}^{2k} \sigma_{ir}^{\alpha} \sigma_{jr}^{\beta} \sigma_{mr}^{\gamma} \right)^2 \tag{17}$$

Note the key difference that this contribution is time-reversal symmetric (i.e. $U = U^{\mathcal{T}}$). As a result of this time-reversal symmetry, this circuit ensemble closely mimics the *circular orthogonal ensemble (COE)* instead of the CUE, producing an extra ground state given by Figure 4. This shifts the mean field treatment as (at O(n)) the Lagrange multipliers are now *quadratically* dependent on the mean fields instead of the *linear* dependence of the pure 2-body case. It also creates competing dynamics between the 2-body and 3-body terms. Intuitively, one would expect a CUE-COE phase transition for the vertical saddle point; we can examine this by considering the singlet eigenvalues in the mixed-body case:

$$\lambda_{\pm} = 6n(J + Mn \pm \sqrt{(2J - 9Mn)^2}) \tag{18}$$

When $\lambda_+ = \lambda_-$, the ground state and first excited state eigenvalues are equal i.e. there is a level crossing; further, recall that when $\lambda_- = 0$, the vertical saddle point represents an stable ground state solution. With some algebra, we can see that we can pick out nontrivial points for both these behaviors of $M = \frac{2J}{9n}$ and $M = \frac{J}{18n}$ respectively. This creates a phase portrait with three regions: one region where 3-body dynamics act as a small perturbation on the 2-body ground states, an intermediate region $\frac{J}{18n} \leq M < \frac{2J}{9n}$ of competing dynamics where the additional 3-body state emerges as a ground state via a phase transition before becoming progressively more excited, and a region where this state's energy is no longer less than that of the lowest 2-body excited state.

Conclusion

Discussion

We have presented a pedagogic explanation of the theoretical workings of the Brownian random circuit model. The simplicity of these methods allows us to compute the noisy XEB at

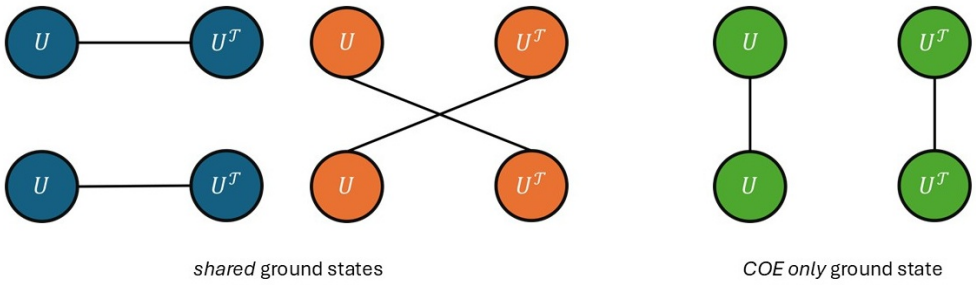

Figure 4: Comparison of the ground states for the CUE and COE. Note that the time-reversal invariance of the latter means $U = U^{\mathcal{T}}$, so the 3-body treatment adds the "vertical" configuration as an additional ground state.

arbitrary depth T and moment k while reproducing the standard results of random matrix theory at infinite depth. Future work will build directly on these results; in the noisy case, this means incorporating channels such as amplitude damping to further model the noise profile of a quantum sampler. We are also exploring applying the Brownian model to higher or arbitrary XEB moments to explore the behavior of these moments under the in the presence of time-reversal invariant interactions and realistic sources of noise. Finally, we will apply this Brownian model to other random circuit procedures - a promising candidate is Bell sampling[14], where a similar simplification of dynamics to this work may allow for analytic results about circuit fidelity that are currently absent from the literature.

Acknowledgments

The authors would like to thank Jasmine Albert, Samuel Bevins, Ryan Cody, and Mohommed Rahman for productive conversations and support with this research. This work is partially supported by the Virginia Space Grant Consortium.

References

[1] Richard P. Feynman. "Simulating physics with computers". en. In: *Int J Theor Phys* 21.6 (June 1982), pp. 467–488. ISSN: 1572-9575. DOI: 10.1007/BF02650179. URL: https://doi.org/10.1007/BF02650179 (visited on 04/06/2026).

[2] John Preskill. "Quantum Computing in the NISQ era and beyond". en. In: *Quantum* 2 (Aug. 2018). arXiv:1801.00862 [quant-ph], p. 79. ISSN: 2521-327X. DOI: 10.22331/q-2018-08-06-79. URL: http://arxiv.org/abs/1801.00862 (visited on 12/15/2025).

[3] Frank Arute et al. "Quantum supremacy using a programmable superconducting processor". en. In: *Nature* 574.7779 (Oct. 2019), pp. 505–510. ISSN: 1476-4687. DOI: 10.1038/s41586-019-1666-5. URL: https://www.nature.com/articles/s41586-019-1666-5 (visited on 12/15/2025).

[4] Sergio Boixo et al. "Characterizing quantum supremacy in near-term devices". en. In: *Nature Phys* 14.6 (June 2018), pp. 595–600. ISSN: 1745-2481. DOI: 10.1038/s41567-018-0124-x. URL: https://www.nature.com/articles/s41567-018-0124-x (visited on 12/15/2025).

[5] Edwin Pednault et al. *Leveraging Secondary Storage to Simulate Deep 54-qubit Sycamore Circuits*. arXiv:1910.09534 [quant-ph]. Oct. 2019. DOI: 10.48550/arXiv.1910.09534. URL: http://arxiv.org/abs/1910.09534 (visited on 12/16/2025).

[6] Xun Gao et al. "Limitations of Linear Cross-Entropy as a Measure for Quantum Advantage". In: *PRX Quantum* 5.1 (Feb. 2024), p. 010334. DOI: 10.1103/PRXQuantum.5.010334. URL: https://link.aps.org/doi/10.1103/PRXQuantum.5.010334 (visited on 12/16/2025).

[7] Gregory Bentsen et al. *On the complexity of sampling from shallow Brownian circuits*. arXiv:2411.04169 [quant-ph]. Nov. 2024. DOI: 10.48550/arXiv.2411.04169. URL: http://arxiv.org/abs/2411.04169 (visited on 12/15/2025).

[8] Gregory S. Bentsen, Subhayan Sahu, and Brian Swingle. "Measurement-induced purification in large-N hybrid Brownian circuits". In: *Phys. Rev. B* 104.9 (Sept. 2021), p. 094304. DOI: 10.1103/PhysRevB.104.094304. URL: https://link.aps.org/doi/10.1103/PhysRevB.104.094304 (visited on 02/25/2026).

[9] Alexios Christopoulos, Amos Chan, and Andrea De Luca. "Universal distributions of overlaps from generic dynamics in quantum many-body systems". In: *Phys. Rev. Res.* 7.4 (Oct. 2025), p. 043035. DOI: 10.1103/kl64-xnsz. URL: https://link.aps.org/doi/10.1103/kl64-xnsz (visited on 04/06/2026).

[10] Pieter W. Claeys and Giuseppe De Tomasi. “Fock-Space Delocalization and the Emergence of the Porter-Thomas Distribution from Dual-Unitary Dynamics”. In: *Phys. Rev. Lett.* 134.5 (Feb. 2025), p. 050405. DOI: 10.1103/PhysRevLett.134.050405. URL: https://link.aps.org/doi/10.1103/PhysRevLett.134.050405 (visited on 04/06/2026).

[11] Scott Aaronson and Lijie Chen. *Complexity-Theoretic Foundations of Quantum Supremacy Experiments*. arXiv:1612.05903 [quant-ph]. Dec. 2016. DOI: 10.48550/arXiv.1612.05903. URL: http://arxiv.org/abs/1612.05903 (visited on 04/06/2026).

[12] Man-Duen Choi. “Completely positive linear maps on complex matrices”. In: *Linear Algebra and its Applications* 10.3 (June 1975), pp. 285–290. ISSN: 0024-3795. DOI: 10.1016/0024-3795(75)90075-0. URL: https://www.sciencedirect.com/science/article/pii/0024379575900750 (visited on 12/15/2025).

[13] Benoit Collins, Sho Matsumoto, and Jonathan Novak. “The Weingarten Calculus”. en. In: *Notices Amer. Math. Soc.* 69.05 (May 2022). arXiv:2109.14890 [math-ph], p. 1. ISSN: 0002-9920, 1088-9477. DOI: 10.1090/noti2474. URL: http://arxiv.org/abs/2109.14890 (visited on 11/29/2025).

[14] Dominik Hangleiter and Michael J. Gullans. “Bell sampling from quantum circuits”. In: *Phys. Rev. Lett.* 133.2 (July 2024). arXiv:2306.00083 [quant-ph], p. 020601. ISSN: 0031-9007, 1079-7114. DOI: 10.1103/PhysRevLett.133.020601. URL: http://arxiv.org/abs/2306.00083 (visited on 02/25/2026).